Supersonic Combustion of a Scramjet Engine Using Hydrogen Fuel in Shock Tunnel

K. Srinivasan,* Praveen K. Maurya,† Kumar Abhishek,‡ S. L. N. Desikan,§ and B. Murugan¶
Vikram Sarabhai Space Centre, Thiruvananthapuram 695 022, India

DOI: 10.2514/1.J056761

Experiments were carried out on a scaled model of scramjet engine with gaseous hydrogen as a fuel in a 1 m combustion-driven shock tunnel. The simulated enthalpy was 2.6 MJ/kg, at a freestream Mach number of 6.8 with varying stagnation pressures (110–190 bar), dynamic pressures (72–130 kPa), and equivalence ratio (0.24–1.16). Detailed studies were carried out to tailor the shock tunnel. Experiments were carried out with air and N_2 as the test gases with hydrogen (H_2) injection to bring out the difference between reactive and nonreactive cases. Pressure measurement along the centerline of the engine and heat flux (through temperature measurements) inside the combustor was carried. The occurrence of supersonic combustion was ascertained through pressure measurements where no upstream influence was seen ahead of the strut injector and the same was corroborated by heat flux measurements. The pressure rise due to supersonic combustion downstream of the fuel injection was nearly three times as compared with nonreactive case. For the current case, when the combustor inlet pressure (P_c) exceeds 1 bar, a sharp rise in the pressure signature was observed downstream of fuel injection, whereas no such marked trace was seen when P_c is below 1 bar.

Downloaded by BIBLIOTHEK DER TU MUENCHEN on July 21, 2018 | http://arc.aiaa.org | DOI: 10.2514/1.J056761

Nomenclature

A	=	area of the injector, m^2
a	=	speed of sound, m/s
C_d	=	coefficient of discharge
C_P	=	coefficient of pressure $(P - P_\infty/q_\infty)$
d_f	=	hydraulic diameter
H	=	enthalpy, J/height of the model, m
h	=	specific enthalpy, J/kg
L	=	length of the model, m
M	=	Mach number
M_c	=	convective Mach number
P	=	pressure, N/m^2
P-L	=	pressure length scale
q	=	dynamic pressure, Pa
T	=	temperature, K
t	=	time, s or ms
U	=	velocity/speed, m/s
W	=	width of the internal duct, mm
X	=	axial distance along the engine from boundary-layer splitter
α	=	thermal diffusivity $(k/\rho\ CP)$/angle of attack, deg
γ	=	ratio of specific heats (C_p/C_v)
ΔQ	=	specific heat addition (J/kg)
η_m	=	mixing efficiency
ρ	=	density, kg/m^3

Subscripts

a	=	air
c	=	combustor
f	=	fuel
i	=	ignition
ij	=	fuel injection properties
m	=	mixture
r	=	chemical reaction
s	=	conditions at surface/at stagnation point/primary shock wave
ϕ	=	equivalence ratio
0	=	stagnation conditions/initial conditions
1	=	initial condition in the driven portion of the shock tube
2	=	condition behind the shock wave
3	=	conditions behind the contact surface
4	=	conditions in the driver tube
5	=	properties in the reflected zone of shock tunnel
∞/ inf	=	freestream conditions

I. Introduction

SUPERSONIC combustion ramjet (scramjet) is being considered as a viable propulsion system for hypersonic vehicles such as missiles and transport passenger vehicles for long-range operation. Further, it is believed to be used as a low-cost access to space in the first stage of two space to orbit (TSTO) vehicles. However, the successfulness of these vehicles depends on the development of efficient propulsion system. As on today, the available propulsion system caters up to $M = 5$, where the turbojet plays a vital role in subsonic and moderate supersonic regimes. On the other hand, ramjet engine is the only solution for $3 \leq M \leq 5$. In both the cases, combustion occurs at subsonic Mach numbers, leads to considerable loss in total pressure, and increases the combustor inlet temperature. As a consequence, the potential to add energy to the flow reduces and the propulsion system can no longer produce significant thrust [1,2]. Hence, to achieve hypersonic Mach numbers ($M > 5$), supersonic combustion ramjet technology is being developed, where the heat is added to the flow at supersonic Mach number, which in turn reduces the combustor inlet temperature so as to propel the vehicle up to $M = 16$. Though the scramjet technology is very attractive, its development mainly depends on efficient fuel-air mixing, ignition, flame holding, its stabilization, and stable combustion owing to millisecond residence time of the supersonic flow inside the combustor.

Many works are carried out in the past to characterize efficient mixing schemes such as injection of fuel normal, oblique, or parallel to the mainstream [3–8]. Though normal injection provides efficient mixing and high level of penetration, the associated total pressure loss is more, which can be reduced substantially through oblique or parallel injection. Several devices are proposed for enhanced mixing

Received 28 September 2017; revision received 28 March 2018; accepted for publication 4 May 2018; published online 16 July 2018. Copyright © 2018 by the American Institute of Aeronautics and Astronautics, Inc. All rights reserved. All requests for copying and permission to reprint should be submitted to CCC at www.copyright.com; employ the ISSN 0001-1452 (print) or 1533-385X (online) to initiate your request. See also AIAA Rights and Permissions www.aiaa.org/randp.

*Wind Tunnel Data Division; k_srinivasan@vssc.gov.in.
†Hypersonic Wind Tunnel Division; pk_maurya@vssc.gov.in, praveenkumariist@gmail.com.
‡Supersonic Wind Tunnel Division; abhishek_kumar@vssc.gov.in.
§Wind Tunnel Data Division; sln_desikan@vssc.gov.in, desikan_sln@yahoo.com (Corresponding Author).
¶Hypersonic Wind Tunnel Division; b_murugan@vssc.gov.in.

Downloaded by BIBLIOTHEK DER TU MUENCHEN on July 21, 2018 | http://arc.aiaa.org | DOI: 10.2514/1.J056761

with reduced total pressure losses, such as ramp mixers [9–12], cavity [13–20], rearward facing step [21–24], pylon [25,26], and strut [27–30]. On the other hand, cavity can also be considered for ignition, flame holding, and stable combustion due to its long residence time and low drag penalty [31], operability range of ignition and blowout limits [32–34], and stable combustion [35–38]. Nevertheless, strut injectors are the most promising candidate because injection of fuel into the core of the main stream leads to rapid and uniform mixing, and its ability on flame holding due to the presence of re-circulation region at the base of the strut.

To achieve supersonic combustion in a typical scramjet engine on ground-based facilities, it is essential to have efficient mixing schemes, thermal management including thermal choking, aerodynamic shaping to reduce the skin friction, and so on [2]. Because of high temperature and pressure, the energy required to duplicate the flight conditions on ground is enormous and is of the order of 100 MW/m^2 [39]. Hence, experiments are carried out in "connected pipe mode," where a supersonic nozzle is used to deliver the required combustion chamber inlet conditions through vitiated air heater. Though this method gives the required conditions for combustor, the uncertainties associated with vitiated air, nonuniformity of the flow during intake, oncoming boundary-layer effect, and the consequence of turbulence need to be studied. These uncertainties can be evaded by direct integration of the supersonic combustor with nozzle, air intake, and isolator with air as a working medium. This is possible in impulse facilities like shock tunnels that can simultaneously generate the required high enthalpy and high pressure [39]. The flowfield inside a scramjet combustor is very complex due to shock-shock and shock wave–boundary layer interactions, turbulent mixing, high-temperature aerothermal chemistry, skin friction drag, and so on, and hence partial ground-based simulation facilities encounter many challenges to predict its performance [2]. Notwithstanding the above limitations, ground test facilities such as shock tunnel play a major role to characterize the flowfield inside the scramjet combustors. Considering the uncertainties involved in the prediction of scramjet flow features, many countries have resorted to small-scale experimental facilities to demonstrate scramjet technology for validating the ground prediction tools. Some of the programs to demonstrate scramjet technology include Kholod of Russia; SCRAM, X43, and X51 of USA; and Hyshot and Scram Space experiments by Australia [40]. However, very limited literature is available on supersonic combustion in a typical scramjet engine at high-enthalpy flows through shock tunnel testing [41–49].

Indian Space Research Organization (ISRO) is embarked upon the development of scramjet technology for low-cost access to space. Toward this, two scramjet engines (engine A and engine B) are attached at the rear portion of a two-stage sounding rocket. Gaseous hydrogen is injected into the combustor through two strut injectors spanning the height of the combustor. On August 28, 2016, at 06:00 hr Indian Standard Time, the sounding rocket booster stage was ignited and the supersonic combustion was demonstrated.

In this context, the present investigation is aimed to demonstrate the occurrence of supersonic combustion in shock tunnel on integrated air intake–isolator–combustor–nozzle configuration. The studies include the tailoring of the shock tunnel, autoignition, and the demonstration of the supersonic combustion through pressure measurements and heat flux (through temperature) measurements.

II. Experimental Details

A. Combustion-Driven Shock Tunnel

The experiments are carried out in 1 m (the maximum nozzle exit diameter that can be used is 1 m) combustion-driven shock tunnel (Fig. 1) at the Vikram Sarabhai Space Centre. The facility consists of a 4-m-long, 0.18-m-internal-diameter driver tube and a 18-m-long, 0.18-m-internal-diameter driven tube. A total of 24 spark plugs are positioned in a double helix fashion in the driver section. Providing the spark plugs in helical fashion [50] ensures uniform spacing both radially and axially, which promotes deflagration mode of combustion. The detonation in shock tunnel occurs through DDT. When the mixture is ignited using a single spark plug and if the L/D is greater than 15, through DDT, detonation occurs. Providing sparks at uniform spacing avoids DDT and ensures deflagration mode of combustion. All the spark plugs are ignited simultaneously to ensure deflagration mode of combustion. A 10° semidivergent conical nozzle having a nozzle exit diameter 0.65 m is used to generate a freestream Mach number of 6.8 ± 0.15 in the test section. The tunnel is designed to generate a maximum enthalpy and a maximum stagnation pressure of 12 MJ/kg and 300 bar, respectively.

B. Scramjet Engine Model and Its Scaling

Scramjet air intake consists of two compression ramps with 10.5° angle followed by two expansion ramps, a cowl, isolator, combustor with two strut configurations having a blockage of 20%, and a single expansion ramp nozzle (SERN). The configuration of the scramjet engine is shown in Fig. 2.

The primary objective of the test is to demonstrate the occurrence of autoignition and supersonic combustion inside the scramjet on the ground. As the runtime in the shock tunnel is ~3 ms, the model scaling should be in such a way to establish the steady flow, mixing, ignition, and combustion within this time period. The time required to establish an attached boundary layer over the model [39,51] is given in Eq. (1).

$$t = \frac{3.3L}{U_\infty} \tag{1}$$

Similarly, the time required for ignition and hydrogen (H_2) reaction [52] is given in Eq. (2):

$$t_i = \frac{8 \times 10^{-9} e^{9600/T}}{P} \tag{2}$$

where P and T are the local pressure and temperature, while the mixture temperature (T_m) of air and hydrogen is related in Eq. (3):

$$T_m = T_a - \frac{0.327\phi}{1 + 0.327\phi}(T_a - T_f) \tag{3}$$

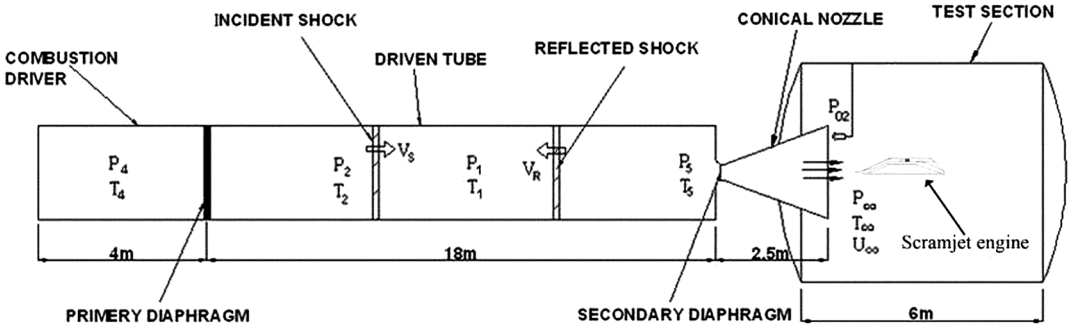

Fig. 1 Schematic of combustion-driven shock tunnel.

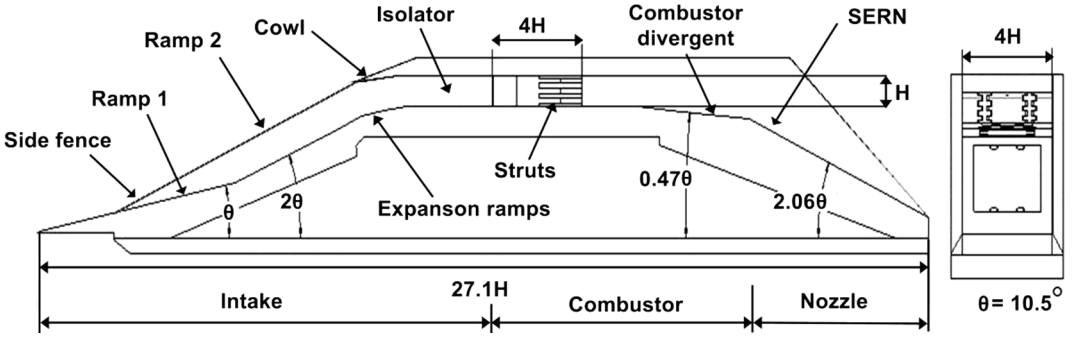

Fig. 2 Details of the scramjet engine.

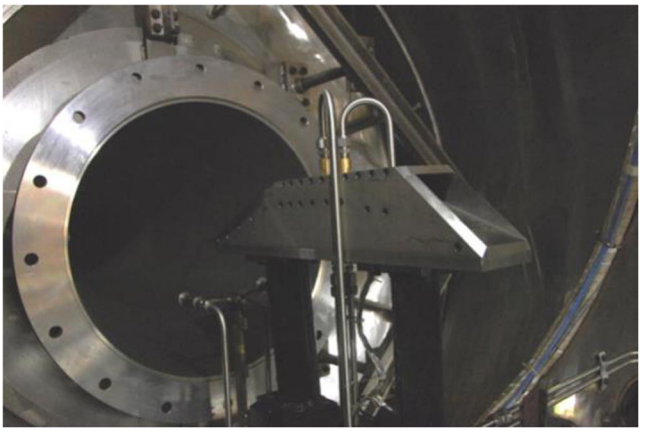

Fig. 3 Model in the test section.

The reaction time [53] is given in Eq. (4):

$$t_r = 1.05 \times 10^{-4} e \frac{-1.12T/1000}{P^{1.7}} \tag{4}$$

The total time for 95% energy release in a constant pressure H_2-air reaction is given by the sum of Eqs. (2) and (4). For an estimated combustion chamber inlet temperature of 1100 K and a precombustion pressure of 1 bar, the time required for ignition and energy release is ∼400 μs. By assuming the freestream velocity of 2000 m/s for a model of 800 mm length, the time to establish a developed flow with attached boundary layer along the model is 1.3 ms [from Eq. (1)]. Thus the total time required to establish the steady flow and combustion is 1.7 ms. Considering the uncertainties in the estimation of runtime, a conservative model scale of 1:3 (length ∼ 800 mm) is chosen and realized. The model is constructed in a modular fashion and is made of stainless steel. The model consists of two side fences, a top plate with cowl, flow duct, fuel injection struts, and a bottom plate. Assembly is made by fastening all the parts using M8, 12.9-grade fasteners, and in the assembled condition the dimensions are checked and assembly integrity is ensured. A photograph of the realized model is shown in Fig. 3.

C. Sensor Locations and Instrumentation

Pressures along the centerline (Fig. 4) of the model at 10 different axial locations are measured using PCB-make piezoelectric pressure transducers (model no: 113B22). The sensor locations are presented in Table 1. The transducers are recess mounted in a cavity of ϕ2 mm × 2 mm (depth) to protect the transducer surface from excessive heat as well as to ensure that the transducers are not protruding into the flow. Heat flux distribution through temperature measurements inside the combustor is done by five numbers of in-house developed E-type co-axial thermocouples with a response time of 2–3 μs [54]. The high-speed data acquisition system consists of National Instruments–based cards for acquiring and storing the pressure and temperature signals. A total of 48 high-speed channels are available for acquiring the test data. Out of 48 channels, 16 channels are used for measuring various parameters (shock speed, P_1, P_2, P_4, P_5, P_{02}, etc.) related to shock tunnel and remaining 32 channels are dedicated for model-associated parameters. To match the analog to digital convert (ADC) card input range, appropriate gains are used and the signals are passed through a Dewetron-make signal conditioner to filter out high-frequency noise. The data are digitized using a 14-bit ADC card stored in the local controller.

D. Simulation Parameters

Apart from Mach number, Reynolds number, and geometry, the important parameters to be simulated for supersonic combustion in impulse facilities are the total enthalpy, the Damkohler numbers, and the wall temperature ratio [49]. Damkohler first and second number simulations ensure that the time scales of reaction and heat added are same between ground facilities and flight. In impulse facilities, the run time is of the order of few milliseconds and scaled-down models are used; it is necessary to use pressure-length (P-L) scaling parameter to establish Damkohler first number. This scaling parameter is valid for scaled-down models [39,52] where binary reactions are involved throughout the flowfield and combustion is mixing dominated [49]. The shock tunnel experiments are carried out at a total enthalpy of 2.6 MJ/kg (to produce intended run time in tunnel). The simulation parameters are presented in Table 2.

E. Freestream Conditions for Scramjet Experiments

The tests are carried out in tailored mode at a stagnation enthalpy of 2.6 MJ/kg with varying primary diaphragms burst pressures (150, 200, and 250 bar) to achieve different tunnel stagnation pressures (110–190 bar). The measured tunnel stagnation conditions and the calculated freestream conditions are presented in Table 3. The stagnant flow expands through a conical nozzle of semidivergent angle of 10° with a throat diameter of 60 mm and an exit diameter of 650 mm. Because the test section Mach number is different from that of the flight, the model is fixed at an angle of 3.5° to mimic flight condition. The hydrogen fuel is injected at choked ($M = 1$) condition

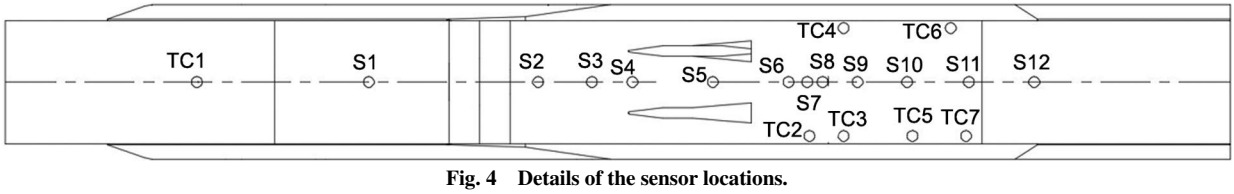

Fig. 4 Details of the sensor locations.

Downloaded by BIBLIOTHEK DER TU MUENCHEN on July 21, 2018 | http://arc.aiaa.org | DOI: 10.2514/1.J056761

with different stagnation pressures (P_{0ij}) varying 7 to 42 bar to get the required equivalence ratio (ER), while the stagnation temperature (T_{0ij}) is maintained at ambient (~300 K) condition.

F. Hydrogen Fuel Injection for Supersonic Combustion

Fuel injection struts A and B are used to supply gaseous H_2 at room temperature (~300 K). Each individual strut is calibrated with H_2 gas for different C_dA values. The experimental setup consists of a pressure source, a pressure-regulating valve, a mass flow meter, and a GP50-make steady pressure transducer to measure the injection pressure. A 2-way pilot-operated, normally closed, explosion-proof solenoid valve with a maximum operating pressure of 350 bar along with 8 mm orifice diameter is used to inject the gaseous H_2. To avoid corruption of the signals, the solenoid valve is kept outside the test section. The gaseous H_2 is supplied from a bank of five commercial-grade hydrogen cylinders to maintain constancy of pressure and temperature during a maximum blow down time of 300 ms. Because of very short runtime, the gas cylinders are charged to the predetermined injection pressure accounting for losses and are operated in a blow down mode. Trial experiments are carried out to study the pressure losses in the fuel injection line and response/

Table 1 Pressure and thermocouple locations on the model

	Sensor locations			Sensor locations	
Sensor, S	X/H	Y/H	Sensor, TC	X/H	Y/H
S1	12.2	0	TC1	6.2	0
S2	17.3	0	TC2	26.2	−1.75H
S3	19.1	0	TC3	27.3	−1.75H
S4	20.4	0	TC4	27.3	1.75H
S5	23.0	0	TC5	29.5	−1.75H
S6	25.5	0	TC6	30.8	1.75H
S7	26.1	0	TC7	31.3	−1.75H
S8	26.6	0			
S9	27.7	0			
S10	29.3	0			
S11	31.3	0			
S12	33.5	0			

S, pressure sensor; TC, thermocouple.

Table 2 Simulation parameters

Parameter	Model
Mach number (M)	6.8
Total pressure (P_0)	110–190 bar
Freestream static pressure (P_∞)	2.2–4.5 kPa
Total enthalpy (H_0)	~2.6 MJ/kg
Freestream static temperature (T_∞)	250 K
Angle of attack	−3.5°
Fuel	Hydrogen
ER	0, 0.24, 0.34, 0.42, 0.63, 0.75, 1.16

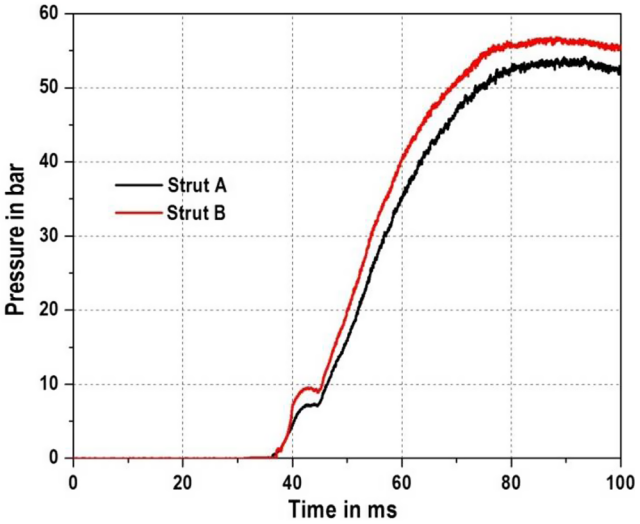

Fig. 5 Response time for various injection pressures.

settling time for various injection pressures (Fig. 5). At $t = 20$ ms, command is given to open the solenoid valve. The trial test indicates that nearly 40–50 ms time is required for the pressure to reach steady value and the pressure loss is different for strut A and strut B (~4bar max). Based on the measured injection pressure and the mass flow rate, C_dA values for strut A and B are 5.36×10^{-6} mm^2 and 4.89×10^{-6} mm^2, respectively. In the actual tests, for different injection pressures, the calibrated value of C_dA is used to calculate H_2 mass flow rate and ER computation.

G. Experimental Procedure

In actual experiments, the command is given to open the H_2 solenoid valve 50 ms before the ignition of combustion driver and the DAQ (Fig. 6) for synchronizing the freestream and the H_2 injection. Because the test section volume is very large (~25 m^3) and is evacuated to ~1 Pa level before the test, H_2 injection before the test with the mass flow rate of 30 g/s has negligible influence on back pressure rise as well as the test results. However, the ratio of fuel injection pressure (P_{0ij}) and freestream pressure (P_∞) plays an important role in mixing.

H. Tailoring the Shock Tunnel

In shock tunnels, the duration of steady test time depends on the arrival of expansion waves/shock wave due to the interaction of the reflected shock with the contact surface or the arrival of the reflected expansion fans from the driver to the reflected zone. To avoid the reflected waves, the acoustic impedance (ρa) across the contact surface needs to be matched. In this process, a Mach wave will be generated owing to the interaction of reflected shock with the contact surface, which ensures uniform flow conditions in the reflected zone. Further to simulate the P-L scaling, a stagnation pressure of >200 bar is required. This necessitates the primary diaphragm burst pressure to

Table 3 Freestream conditions for scramjet tests

Run No.	P_4, bar	P_1, mbar	U_S, m/s	P_5, bar	h_5, MJ/kg	P_{02}, bar	P_c, bar	ER	P_∞, kPa	T_∞, K	U_∞, m/s	ρ_∞, kg/m^3
542	277	1218	1530	166	2.7	2.172	1.6	0.42	3.53	261.5	2207	4.7E − 02
543[a]	250	1190	1668	155	2.92	2.15	1.5	N_2/H_2	3.66	293.8	2292	4.3e − 02
544	250	1210	1562	150	2.68	1.78	1.5	0.24	2.76	249.2	2206	3.7e − 02
545	200	900	1620	111	2.79	1.26	1	0.32	1.91	253.8	2250	2.6e − 02
546[b]	55	510	1252	37	1.84	0.53	0.28	0.00	0.85	174.5	1822	1.7e − 2
550[c]	250	1200	1644	177	2.98	2.22	1.4	0.53	3.59	288	2320	4.4e − 02
551	300	1600	1520	190	2.58	2.45	1.5	0.63	3.94	247.6	2157	5.6e − 02
552	220	1250	1498	140	2.49	1.86	1.25	0.75	3.10	240.7	2122	4.4e − 02
556	250	1575	1421	170	2.34	2.21	1.5	1.16	3.55	223.4	2055	5.5e − 02

[a]No reaction.
[b]No injection.
[c]No combustion.

Downloaded by BIBLIOTHEK DER TU MUENCHEN on July 21, 2018 | http://arc.aiaa.org | DOI: 10.2514/1.J056761

Downloaded by BIBLIOTHEK DER TU MUENCHEN on July 21, 2018 | http://arc.aiaa.org | DOI: 10.2514/1.J056761

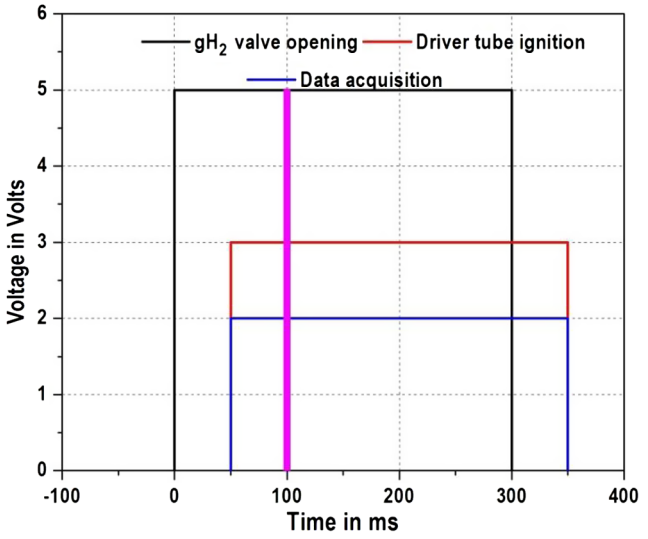

Fig. 6 Operation sequence of H_2 injection and the freestream.

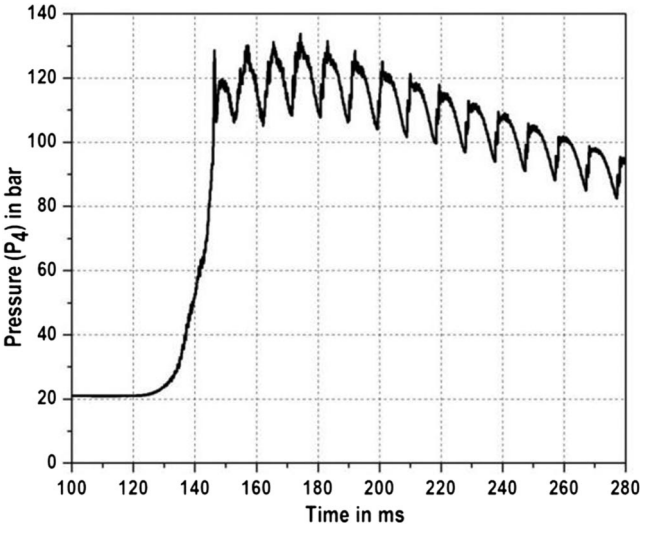

Fig. 7 Pressure history inside the combustion driver tube for constant volume.

be in excess of 250 bar. Thus, apart from generating adequate runtime, the goal of the tailoring is to get a postcombustion pressure around 300 bar in the combustion driver so as to produce the required P_5. Tailoring of the shock tunnel is achieved by diluting the stoichiometric mixture of oxygen and hydrogen with diluents such as helium (He), argon (Ar), and nitrogen (N_2) in different volumetric proportions. This is done in the present studies in which the driver section is filled with gas mixture along with the diluents and ignited simultaneously. To measure the postcombustion speed of sound (a_4), the primary diaphragm is not allowed to rupture so that the combustion occurs at constant volume. As a result, a sudden pressure rise occurs, which leads to the formation of a standing pressure wave in the driver section, which is measured by a PCB pressure sensor. The pressure history of a typical gas mixture ratio of 1.1:2:9 (oxygen: hydrogen:argon [O_2:H_2:Ar]) presented in Fig. 7 shows cyclic oscillations (frequency of oscillation is 114 Hz) after reaching the maximum value. It is assumed that the pressure wave is stationary with its fundamental tone. The fast Fourier transform (FFT) of the pressure signal presented in Fig. 8 shows that the fundamental mode (114 Hz) is dominant. The two closed ends of the driver section become the nodes for the standing wave, and half of the wavelength of the wave is equal to the length of the tube. In this way a_4 is calculated for all the gas mixtures and are presented in Table 4.

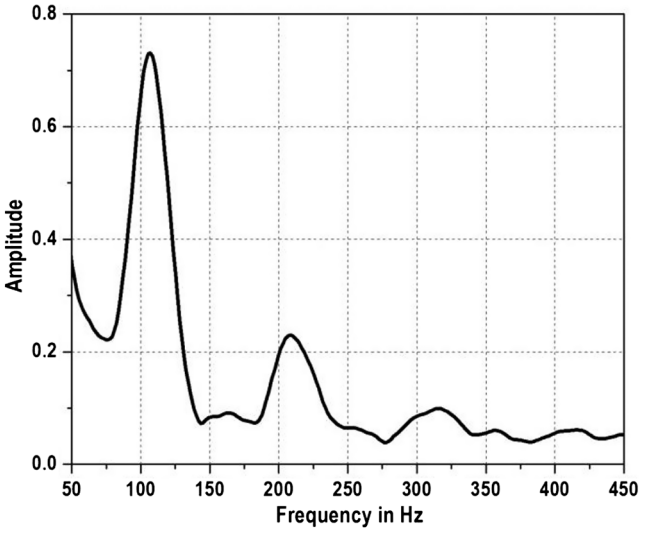

Fig. 8 FFT of the pressure signal.

The first gas mixture (case A in Table 4) is tested with argon dilution in the stoichiometric mixture of hydrogen and oxygen for two diaphragm pressures (150 and 200 bar). Argon is added in the mixture to reduce postcombustion speed of sound (a_4), whereas 10% more oxygen is added to ensure complete combustion of hydrogen to avoid interface combustion at the contact surface [55]. Though case A (150 bar) is found to be suitable in terms of a_4 and runtime (~3 ms), it produces lower value of P_5 (Fig. 9) due to the attenuation of shock speed during the test owing to higher molecular weight of the driver gas. For higher diaphragm pressures (200 bar), the attenuation of shock speed further increases and the runtime is not sufficient. This is valid for the cases B and C. Hence, N_2 gas dilution (case D in Table 4) is used to get the run time of 3 ms. However, at higher loading pressures, the combustion takes long time and in many tests the combustion is not repeatable.

Hence, a new mixture (cases E and F in Table 4) of He and Ar is tested for combustion at higher loading pressures to get a_4 of ~1000 m/s. The new mixture (case E) takes more than 500 ms for a loading pressure of ~30 bar, whereas for case *H* it is ~150 ms for ~40 bar loading pressure. Since the rise in time is large due to heat loss (to the walls of the combustion driver), intended pressure jump could not be achieved. The reason could be higher dilution of the gases. Hence, the ratio of diluents is reduced to 9 parts (case G, Table 4) with He and Ar in the volumetric ratio of 5 and 4, respectively. As a result, higher a_4 (~1120 m/s) in the driver is achieved but the mixture is combusting for filling pressure up to ~45 bar and produces a postcombustion pressure of ~300 bar (Fig. 10). Though the goal of tailoring is to get an enthalpy of ~1.7 MJ/kg for P_5 of ~200 bars, the same could not be achieved with the cases A–F and hence the mixture case G is selected, which can produce a runtime >3 ms and a P_5 of ~200 bars. Because the mixture case G has a high postcombustion speed of sound (a_4), the tunnel could be tailored only at a high enthalpy of ~2.6 MJ/kg. A typical P_5 traces for mixture case I depicting the run time >3 ms for various diaphragm pressures are shown in Fig. 11.

Table 4 Gas mixture ratios (volumetric) for tunnel tailoring

Case	O_2	H_2	He	Ar	N_2	a_4, m/s
A	1.1	2		9		880
B	1.1	2		10		840
C	1.1	2		7		888
D	1.1	2	2		5	1000
E	1.1	2	7	6		1000
F	1.1	2	6	5		1080
G	1.1	2	5	4		1120

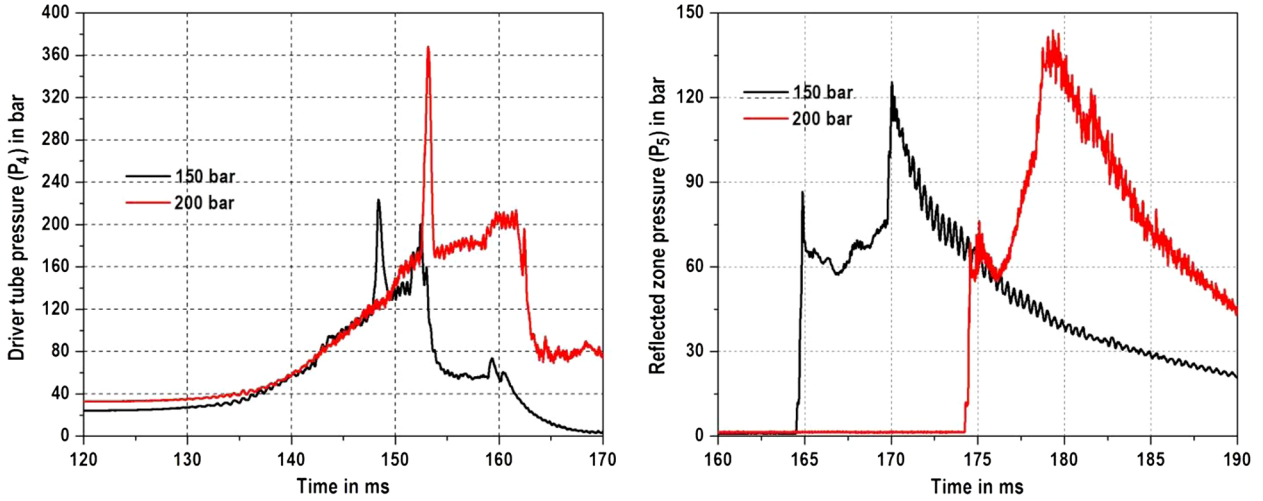

Fig. 9 Pressure traces in the driver tube and reflected zone (case A of Table 4).

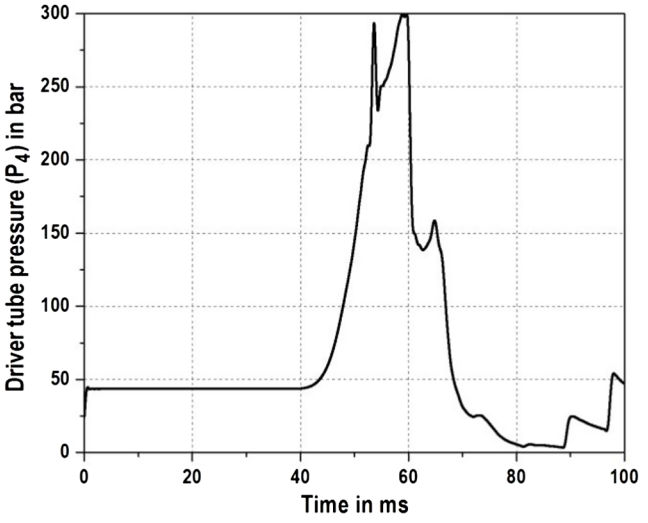

Fig. 10 Pressure trace in the driver tube for helium-argon mixture (case G, Table 4).

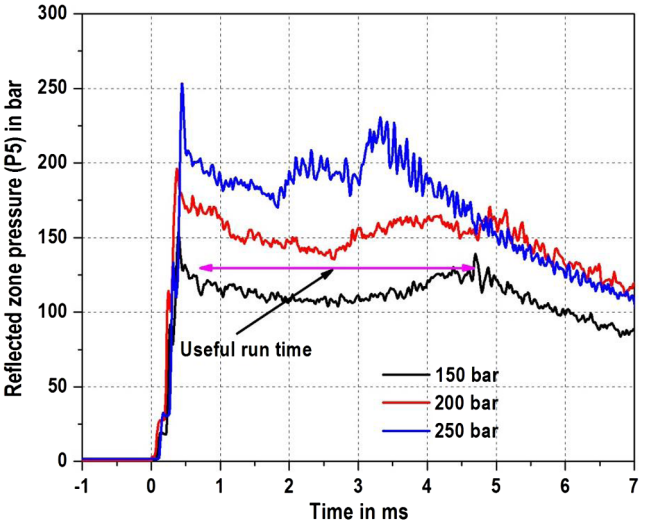

Fig. 11 Typical P_5 trace for the scramjet experiments.

III. Results and Discussion

Shock tunnel tests are carried out for the three conditions, namely, tests with primary air alone (Case H, Run No. 546), tests with N_2 as the primary flow with H_2 injection (case I, Run No. 543), and tests with air as primary flow at different dynamic pressures with H_2 injection (case J, Run No. 542) for various ER. To ascertain the occurrence of supersonic combustion, pressure measurement along the centerline of the model is compared for the test cases H, I, and J in Table 5.

The nondimensional pressure distribution for cases H, I, and J matches till the fuel injection strut for all the three cases. On the other hand, a small pressure rise due to secondary gas injection is seen behind the strut for case I, and approximately three times pressure rise due to combustion for case J is observed. The absence of upstream interaction and large pressure rise after the strut for case J confirms the occurrence of supersonic combustion. Heat flux measurements in the combustor are also carried out to complement the pressure data (Fig. 12). The heat flux (Fig. 13) is highest at all locations for case J as compared with cases H and I, thus corroborating the pressure measurements and confirming the occurrence of supersonic combustion. The present measurements are in line with the heat flux measurement reported in the literature [40,56], where the d ratio of heat flux for fuel-on (reacting) and fuel-off condition is observed to be ~2 times.

A. Ignition and Mixing Delay

A typical pressure trace at $x/H = 26.1$ just behind the strut is shown in Fig. 14 for both with and without combustion. It can be observed that nearly 0.6 ms is required for the flow to stabilize and further ~0.4 ms is taken for the combustion to occur; that is, mixing plus ignition delay time combined is ~1.1 ms. However, on the other hand, additionally 0.6 ms is needed to raise pressure to the maximum value. Here it can be observed that the total rise time for pressure due to combustion is ~1.7 ms, which is in line with the empirical value as discussed earlier.

B. Effect of Equivalence Ratio (ER)

The ER is varied from 0.24 to 1.16 by changing the fuel injection pressure (P_{0ij}) and freestream conditions. Nondimensional pressure (C_p) distribution along the centerline of the engine is plotted and compared for different ERs in Fig. 15. The location of first pressure

Table 5 Test conditions to confirm the occurrence of supersonic combustion

Run No.	Test gas	P_5, bar	Hydrogen, g/s	Enthalpy, MJ/kg	Remark
546	Air	37	No injection	1.80	Case H
543	N_2	155	9.73	2.92	Case I
542	Air	166	8.72	2.70	Case J

Downloaded by BIBLIOTHEK DER TU MUENCHEN on July 21, 2018 | http://arc.aiaa.org | DOI: 10.2514/1.J056761

Downloaded by BIBLIOTHEK DER TU MUENCHEN on July 21, 2018 | http://arc.aiaa.org | DOI: 10.2514/1.J056761

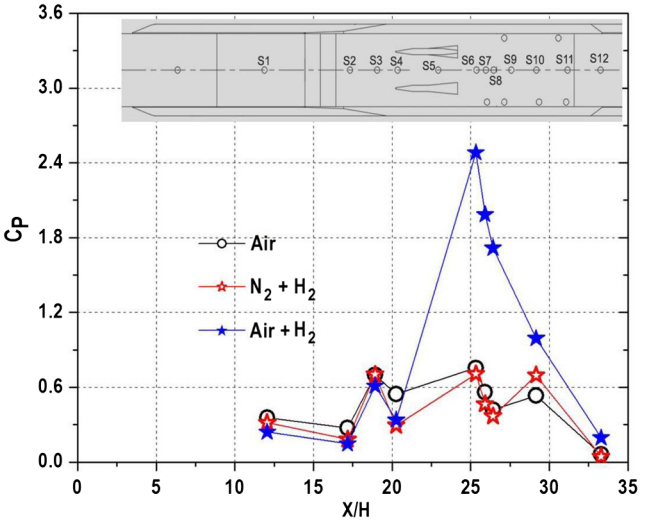

Fig. 12 Pressure distribution inside the engine.

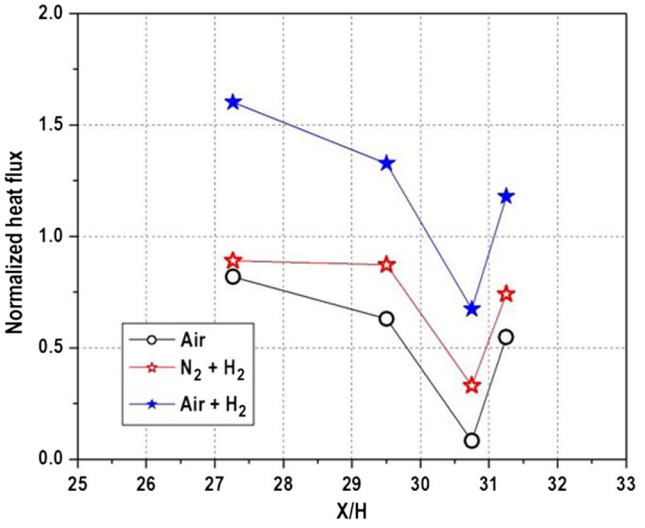

Fig. 13 Heat flux distribution inside the engine.

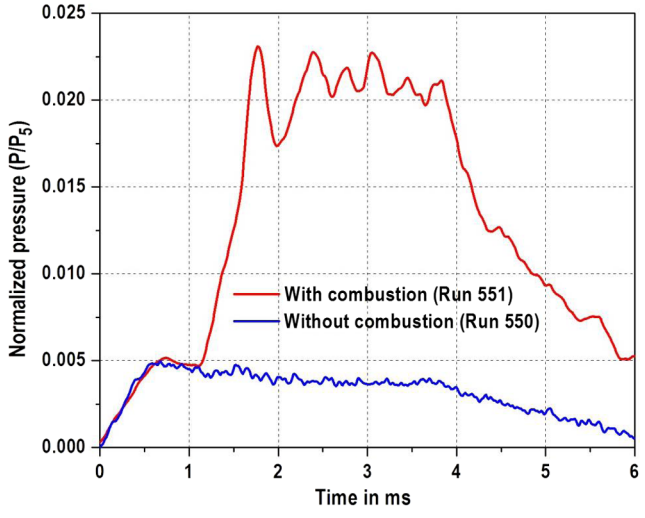

Fig. 14 Ignition and mixing delay time.

sensor after the fuel injection point, that is, end of strut, is $x/H = 25.5$ and designated as sensor S6 as shown in Fig. 5 and Table 1. When ER is increased, as anticipated, rise in pressure (ΔP) due to combustion increases and a maximum C_p of 3.2 is observed. For ER of 0.24, noticeable rise in pressure could be observed only at the S8 pressure sensor located after the strut end, whereas for ER of 0.34 the pressure rise could be observed from the sensor S7 onward, whereas for ER of 0.41 and above, the ignition starts occurring immediately from the sensor S6 after the strut. This could mean that the ignition delay and mixing length are more for low ER. An approximate expression for combustion pressure rise is given by Eq. (5) [3].

$$\frac{P_C}{P_1} = \frac{1 + (\gamma - 1)\Delta Q}{a^2} \tag{5}$$

With $\Delta Q = 3.5$ MJ/kg, $\gamma = 1.3$, and a precombustion temperature of 1100 K, P_c/P_1 is 3.55 and the same is also observed from the present experiments. Results further indicate that up to an ER 1.16, no upstream interaction is present and the combustion occurs at supersonic mode. The normalized heat flux measurements also corroborated the occurrence of combustion. As expected with the increase in ER, the heat flux also increases (Fig. 15).

C. Effect of Combustor Inlet Static Pressure (P_c)

It is observed that when the static pressure in the combustion chamber is less than 1 bar, pressure rise is not observed close to the strut injection location irrespective of the ER. Rather, it occurs beyond X/H of 27.7 (sensor S9) as shown in Fig. 16. This is also evident from heat flux measurement where the rise in heat flux is seen at this point. The obtained results are in line with the literature [40,57]. In this, when combustion chamber inlet pressure is 1.3 bar, immediate rise in the pressure is seen just downstream of the fuel injection location due to combustion. On the other hand, for P_c of 0.57 bar the rise in pressure is observed at ~100 mm downstream of the fuel injection location due to combustion.

The empirical formula for mixing length for struts in supersonic flow is given in Eqs. (6) and (7) [58].

$$M_c = \frac{(U_f - U_a)}{(a_f + a_a)} \frac{L_m}{d_f} = \frac{K^*}{f(M_c)} \left\{ \frac{\rho_f u_f}{\rho_c u_c} \right\}^{0.5} \tag{6}$$

$$f(M_c) = 0.25 + 0.75(e^{-3M_c^2})\eta_m = a(1 - e^{-(k\bar{x})^{d_f}}) \tag{7}$$

where $a = 1.06492$, $k = 3.69639$, $K^* = 390$, and $d = 0.80586$ are constants, and η_m, M_c, and d_f are the mixing efficiency, the convective Mach number, and the hydraulic diameter, respectively. From the above model, it can be observed that reducing the momentum of the air leads to large mixing length, which in turn leads to increase the pressure due to combustion as observed in the experiments. Further, it is reported that at lower combustor static pressures, H_2 and O_2 reaction produces OH^- and H^+ in the first step and recombination to produce H_2O happens slowly and further downstream of the strut, whereas at higher combustor inlet static pressures, the recombination happens quickly and H_2O conversion happens immediately downstream of the strut [53], which may also be a cause for this behavior. Table 6 summarizes the combustion chamber inlet pressure.

D. Effect of Runtime

In the present series of tests the enthalpy is varied from 1.7 to 2.6 MJ/kg. When the tests are carried at low enthalpy (1.7 MJ/kg), supersonic combustion is not achieved. This is probably due to lower runtime in the facility. Hence, to ensure proper runtime, tests are carried out at 2.6 MJ/kg and the results show the supersonic combustion. Therefore it is essential that when carrying out tests at lower enthalpy like 1.7 MJ/kg, a driver gas that can produce a minimum runtime of 4–5 ms is preferable.

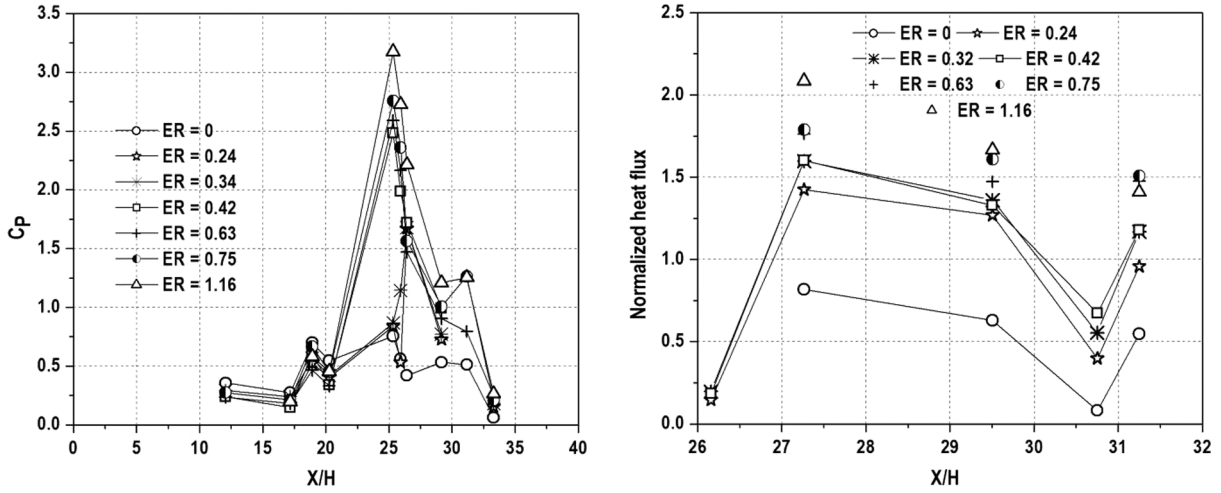

Fig. 15 Centerline pressure distribution and normalized heat flux variation for various ERs.

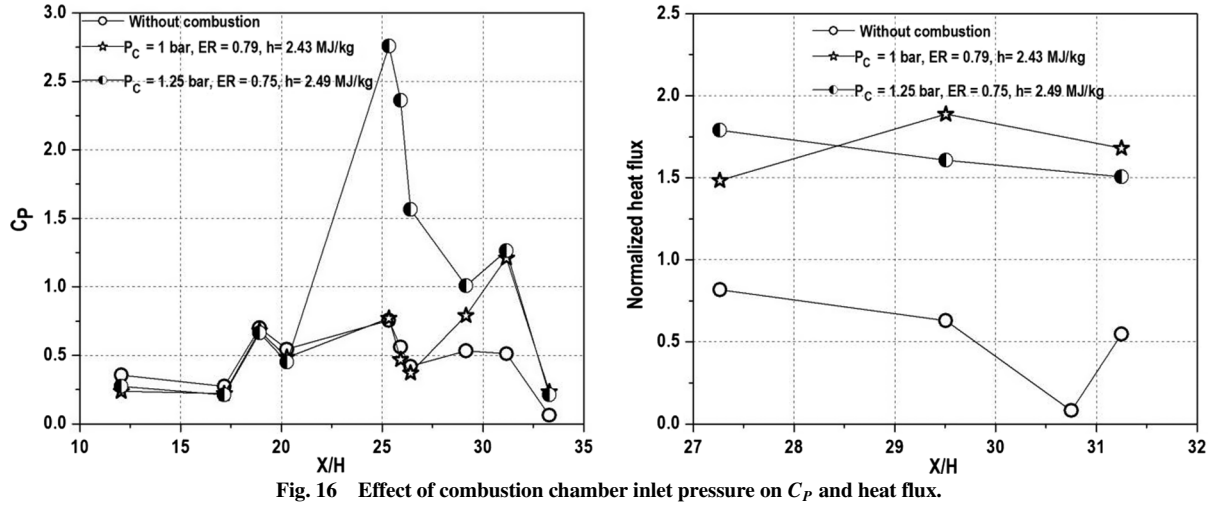

Fig. 16 Effect of combustion chamber inlet pressure on C_P and heat flux.

E. Measurement Uncertainty

1. Error in the Estimation of ER

Based on the C_dA values, error in the estimation of ER is $\pm 2\%$. The error in the pressure values measured by PCB sensor is $\pm 1\%$, while the error in the estimation of percentage of the captured mass flow rate by the engine is $\pm 5\%$. Therefore the overall error in the estimation of the ER is calculated to be $\pm 5.5\%$ (2σ).

2. Error in Pressure and Heat Flux Measurement

To demonstrate the repeatability of the data, two tests are carried out for similar ER and presented in Fig. 17. From the figure, it can be observed that the repeatability is very good and the data match within 1%. As the repeatability alone is not a measure of uncertainty, errors associated with P_1, T_1, P_2, U_s, P, and P_{02} measurements are calculated using the method of propagation of errors. Based on methodology [56], typical uncertainty in C_p measurement is estimated to be $\pm 12\%$, whereas for heat flux it is $\pm 15\%$.

Table 6 Effect of combustion chamber inlet pressure

Run No.	P_5/P_c, bar	ER	Enthalpy, MJ/kg	Remark
552	140/1.25	0.75	2.49	Combustion
553	120/0.95	0.79	2.43	Combustion not captured by pressure measurements

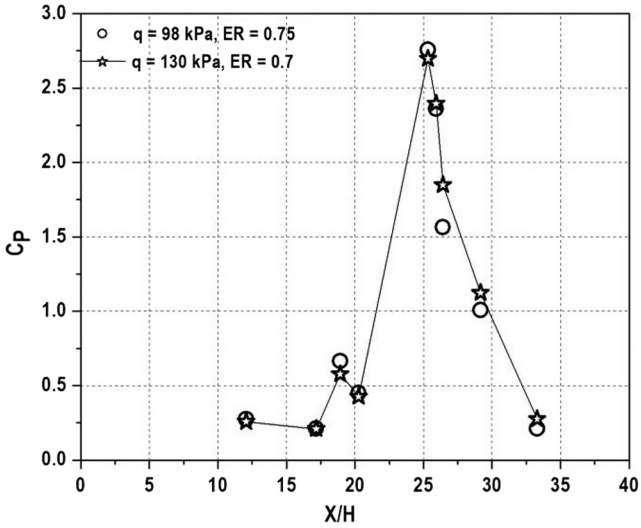

Fig. 17 Repeatability of test data.

IV. Conclusions

Experiments are carried out in the shock tunnel to demonstrate autoignition and supersonic combustion in a scramjet engine. Extensive studies are carried out to tailor the shock tunnel to cater for the flight enthalpy. In this, by diluting the stoichiometric mixture of

Downloaded by BIBLIOTHEK DER TU MUENCHEN on July 21, 2018 | http://arc.aiaa.org | DOI: 10.2514/1.J056761

oxygen and hydrogen with diluents such as He, Ar, and N_2 in different volumetric proportions in the driver section, tailoring of the tunnel is achieved. Also, the flow establishment time of 0.6 ms and the combined flow establishment, mixing, and ignition delay time of 1.1 ms in the tunnel are demonstrated since the tunnel run time is of the order of 3 ms. The occurrence of the supersonic combustion for different equivalence ratio (ER) is studied through pressure and temperature measurements. The supersonic combustion is confirmed through no upstream influence ahead of the injection points through pressure measurements, which are corroborated through heat flux derived from the temperature measurements. For ER between 0.72 to 1.16, the peak pressure due to supersonic combustion is found to be 3–4 times the nonreactive case. On the other hand, once the combustion chamber entry pressure (P_c) is reduced below 1 bar it leads to an increase in the mixing length, which in turn shifts the peak pressure due to the occurrence of combustion much downstream of the strut.

Acknowledgements

The authors would like to thank R. Saravanan, Noorul Ameen, and Binoy Mathew from the Hypersonic Wind Tunnel Division for their unbound support in carrying out the experiments.

References

[1] Falempin, F., "Ramjet and Dual Mode Operation," *Advances on Propulsion Technology for High-Speed Aircraft*, Paper 7, Educational Notes RTO-EN-AVT-150, Neuilly-sur-Seine, France, 2008, pp. 7.1–7.36, http://www.rto.nato.int.

[2] Smart, M., "Scramjets," *Advances on Propulsion Technology for High-Speed Aircraft*, Educational Notes RTO-EN-AVT-150, 2008, pp. 9.1–9.38.

[3] Zukoski, E. E., and Spaid, F. W., "Secondary Injection of Gases into a Supersonic Flow," *AIAA Journal*, Vol. 2, No. 10, 1964, pp. 1689–1696. doi:10.2514/3.2653

[4] Billig, F. S., Orth, R. C., and Lasky, M. A., "Unified Analysis of Gaseous Jet Penetration," *AIAA Journal*, Vol. 9, No. 6, 1971, pp. 1048–1058. doi:10.2514/3.49916

[5] Vanlerberghe, W. M., Santiago, J. G., Dutton, J. C., and Lucht, R. P., "Mixing of a Sonic Transverse Jet Injected into a Supersonic Flow," *AIAA Journal*, Vol. 38, No. 3, 2000, pp. 470–479. doi:10.2514/2.984

[6] Papamoschou, D., and Hubbard, D. G., "Visual Observations of Supersonic Transverse Jets," *Experiments in Fluids*, Vol. 14, No. 6, 1993, pp. 468–476. doi:10.1007/BF00190201

[7] Gruber, M. R., Nejad, A. S., Chen, T. H., and Dutton, J. C., "Mixing and Penetration Studies of Sonic Jets in a Mach 2 Freestream," *Journal of Propulsion and Power*, Vol. 11, No. 2, 1995, pp. 315–323. doi:10.2514/3.51427

[8] Hartfield, R. J., and Bayley, D. J., "Experimental Investigation of Angled Injection in Compressible Flow," *Journal of Propulsion and Power*, Vol. 12, No. 2, 1996, pp. 442–445. doi:10.2514/3.24054

[9] Waitz, I. A., Marble, F. E., and Zukoski, E. E., "Vorticity Generation by Contoured Wall Injectors," AIAA Paper 1992-3550, 1992. doi:10.2514/6.1992-3550

[10] Stouffer, S. D., Baker, N. R., Capriotti, D. P., and Northam, G. B., "Effects of Compression and Expansion Ramp Fuel Injector Configurations on Scramjet Combustion and Heat Transfer," AIAA Paper 1993-0609, 1993. doi:10.2514/6.1993-609

[11] Hartfield, R. J., Hollo, S. D., and Mcdaniel, J. C., "Experimental Investigation of a Supersonic Swept Ramp Injector Using Laser Induced Iodine Fluorescence," *Journal of Propulsion and Power*, Vol. 10, No. 1, 1994, pp. 129–135. doi:10.2514/3.23721

[12] Wilson, M. P., Bowersox, R. W. D., and Glawe, D. D., "Experimental Investigation of the Role of Downstream Ramps on a Supersonic Injection Plume," *Journal of Propulsion and Power*, Vol. 15, No. 3, 1999, pp. 432–439. doi:10.2514/2.5462

[13] Kumar, A., Bushnell, D. M., and Hussaini, M. Y., "Mixing Augmentation Technique for Hypervelocity Scramjet," *Journal of Propulsion and Power*, Vol. 5, No. 5, 1989, pp. 514–522. doi:10.2514/3.23184

[14] Zang, X., and Edwards, J. A., "An Investigation of Supersonic Oscillatory Cavity Flows Driven by Thick Shear Layers," *The Aeronautical Journal*, Vol. 94, No. 940, 1990, pp. 355–364. doi:10.1017/S0001924000023319

[15] Yu, K. H., and Schadow, K. C., "Cavity-Actuated Supersonic Mixing and Combustion Control," *Combustion and Flame*, Vol. 99, No. 2, 1994, pp. 295–301. doi:10.1016/0010-2180(94)90134-1

[16] Sato, N., Imamura, A., Shiba, S., Takahashi, S., Tsue, M., and Kono, M., "Advanced Mixing Control in Supersonic Airstream with a Wall-Mounted Cavity," *Journal of Propulsion and Power*, Vol. 15, No. 2, 1999, pp. 358–360. doi:10.2514/2.5433

[17] Mohamed Ali, M. C., and Kurian, J., "Cavity-Based Injections into Supersonic Flow," *Journal of Propulsion and Power*, Vol. 21, No. 6, 2005, pp. 1130–1132. doi:10.2514/1.15716

[18] Grady, N. R., Pitz, R. W., Carter, C. D., Hsu, K. Y., Ghodke, C., and Menon, S., "Supersonic Flow over a Ramped-Wall Cavity Flame Holder with an Upstream Strut," *Journal of Propulsion and Power*, Vol. 28, No. 5, 2012, pp. 982–990. doi:10.2514/1.B34394

[19] Moorthy, J. V. S., Rajinikanth, B., Charyulu, B. V. N., and Amba Prasad Rao, G., "Effect of Ramp-Cavity on Hydrogen Fueled Scramjet Combustor," *Journal of Propulsion and Power Research*, Vol. 3, No. 1, 2014, pp. 22–28. doi:10.1016/j.jppr.2014.01.001

[20] Rasmussen, C. C., Driscoll, J. F., Carter, C. D., and Hsu, K. Y., "Characteristics of Cavity Stabilized Flames in a Supersonic Flow," *Journal of Propulsion and Power*, Vol. 21, No. 4, 2005, pp. 765–768. doi:10.2514/1.15095

[21] Karagozian, A. R., Wang, K. C., Lee, A. T., and Smith, O. I., "Transverse Gas Injection Behind a Rearward Facing Step," *Journal of Propulsion and Power*, Vol. 12, No. 6, 1996, pp. 1129–1136. doi:10.2514/3.24153

[22] Bogdanoff, D. W., "Advanced Injection and Mixing Techniques for Scramjet Combustors," *Journal of Propulsion and Power*, Vol. 10, No. 2, 1994, pp. 183–190. doi:10.2514/3.23728

[23] Gruenig, C., Avrashkov, V., and Mayinger, F., "Fuel Injection into a Supersonic Airflow by Means of Pylons," *Journal of Propulsion and Power*, Vol. 16, No. 1, 2000, pp. 29–34. doi:10.2514/2.5560

[24] Masuya, G., Komuro, T., Murakami, A., Shinozaki, N., Nakamura, A., Murayama, M., and Ohwaki, K., "Ignition and Combustion Performance of Scramjet Combustors with Fuel Injection Struts," *Journal of Propulsion and Power*, Vol. 11, No. 2, 1995, pp. 301–307. doi:10.2514/3.51425

[25] Sunami, T., Murakami, A., Kudou, K., Nishioka, M., and Wendt, M. N., "Alternating Wedge Strut Injection for Supersonic Mixing and Combustion," *Fourteenth International Symposium on Air Breathing Engines*, AIAA, Reston, VA, Sept. 1999.

[26] Desikan, S. L. N., and Kurian, J., "Strut-Based Gaseous Injection into a Supersonic Stream," *Journal of Propulsion and Power*, Vol. 22, No. 2, 2006, pp. 474–477. doi:10.2514/1.16770

[27] Desikan, S. L. N., and Kurian, J., "Mixing Studies in Supersonic Flow Employing Strut Based Hypermixers," AIAA Paper 2005-3643, 2005. doi:10.2514/6.2005-3643

[28] Fox, J. S., Gaston, M. J., Houwing, A. F. P., and Danehy, P. M., "Comparison of Hypermixing Injectors Using a Mixture-Fraction-Sensitive Imaging Technique," *Proceedings of the Thirteenth Australasian Fluid Mechanics Conference*, edited by M. C. Thompson, and K. Hourigan, Vol. 1, Monash Univ., Melbourne, Australia, Dec. 1998, pp. 79–82.

[29] Desikan, S. L. N., and Kurian, J., "Experimental Investigation of the Role of Struts in High Speed Mixing," *The Aeronautical Journal*, Vol. 117, No. 1188, 2013, pp. 193–211. doi:10.1017/S0001924000007946

[30] Desikan, S. L. N., Kumaran, K., and Babu, V., "Numerical Investigation of the Role of Hyper-Mixers in Supersonic Mixing," *The Aeronautical Journal*, Vol. 114, No. 1161, 2010, pp. 659–672. doi:10.1017/S0001924000004140

[31] Gruber, M. R., Donbar, J. M., Carter, C. D., and Hsu, K. Y., "Mixing and Combustion Studies Using Cavity-Based Flame-Holders in a Supersonic Flow," *Journal of Propulsion and Power*, Vol. 20, No. 5, 2004, pp. 769–778. doi:10.2514/1.5360

Downloaded by BIBLIOTHEK DER TU MUENCHEN on July 21, 2018 | http://arc.aiaa.org | DOI: 10.2514/1.J056761

[32] Mathur, T., Gruber, M., Jackson, K., Donbar, J., Donaldson, W., Jackson, T., and Billing, F., "Supersonic Combustion Experiments with a Cavity-Based Fuel Injector," *Journal of Propulsion and Power*, Vol. 17, No. 6, 2001, pp. 1305–1312. doi:10.2514/2.5879

[33] Ben-Yakar, A., and Hanson, R. K., "Cavity Flame-Holders for Ignition and Flame Stabilization in Scramjets: An Overview," *Journal of Propulsion and Power*, Vol. 17, No. 4, 2001, pp. 869–877. doi:10.2514/2.5818

[34] Kim, K. M., Baek, S. W., and Han, C. Y., "Numerical Study on Supersonic Combustion with Cavity-Based Fuel Injection," *International Journal of Heat and Mass Transfer*, Vol. 47, No. 2, 2004, pp. 271–286. doi:10.1016/j.ijheatmasstransfer.2003.07.004

[35] Gu, H. B., Chen, G. L., and Chang, X. Y., "Experimental Investigation of Cavity-Based Scramjet Model," AIAA Paper 2006-7917, 2006. doi:10.2514/6.2006-7917

[36] Freeborn, A. B., King, P. I., and Gruber, M. R., "Swept-Leading-Edge Pylon Effects on a Scramjet Pylon-Cavity Flameholder Flow Field," *Journal of Propulsion and Power*, Vol. 25, No. 3, 2009, pp. 571–582. doi:10.2514/1.39546

[37] Huang, W., Pourkashanian, M., Ma, L., Ingham, D. B., Luo, S. B., and Wang, Z. G., "Investigation on the Flame Holding Mechanisms in Supersonic Flows: Backward-Facing Step and Cavity Flame-holder," *Journal of Flow Visualization*, Vol. 14, No. 1, 2011, pp. 63–74. doi:10.1007/s12650-010-0064-8

[38] Bao, H., Zhou, J., Pan, Y., and Wang, S., "Spark Ignition of Liquid Kerosene in Scramjet Combustor Equipped with Partly-Covered Cavity," *Journal of Propulsion and Power*, Vol. 31, No. 4, 2015, pp. 1014–1018. doi:10.2514/1.B35469

[39] Stalker, R. J., "Scramjets and Shock Tunnels—The Queensland Experience," *Progress in Aerospace Sciences*, Vol. 41, No. 6, 2005, pp. 471–513. doi:10.1016/j.paerosci.2005.08.002

[40] Curran, E. T., and Murthy, S. N. B., *Scramjet Propulsion*, Progress in Astronautics and Aeronautics, Vol. 189, AIAA, Reston, VA, 2000. doi:10.2514/4.866609

[41] Osgerby, I. T., Smithson, H. K., and Wagner, D. A., "Development of a Double-Oblique Shock Scramjet Model in a Shock Tunnel," *Journal of Aircraft*, Vol. 8, No. 4, 1971, pp. 258–263. doi:10.2514/3.44265

[42] Rogers, R. C., Shih, A. T., and Hass, N. E., "Scramjet Development Tests Supporting the Mach 10 Flight of the X-43," AIAA Paper 2005-3351, 2005. doi:10.2514/6.2005-3351

[43] Gardner, A. D., Hannemann, K., Paull, A., and Steelant, J., "Post Flight Analysis of the HYSHOT Supersonic Combustion Flight Experiment in HEG," *Proceedings of the 5th European Symposium of Aerothermodynamics for Space Vehicles*, edited by D. Danesy, ESA Publ., Noordwijk, The Netherlands, Nov. 2004.

[44] Tanno, H., Itoh, K., and Ueda, S., "Scramjet Testing in High Enthalpy Shock Tunnel (HIEST)," Ramjet Propulsion Research Center, Japan Aerospace Exploration Agency (JAXA), Japan, 2017, pp. 120–124.

[45] Kang, S. H., Lee, Y. K., Yang, S. S., Smart, M. K., and Suraweera, M. V., "Cowl and Cavity Effects on Mixing and Combustion in Scramjet Engines," *Journal of Propulsion and Power*, Vol. 27, No. 6, 2011, pp. 1169–1177. doi:10.2514/1.48818

[46] McGilvray, M., Kirchhartz, R., and Jazra, T., "Comparison of Mach 10 Scramjet Measurements from Different Impulse Facilities," *AIAA Journal*, Vol. 48, No. 8, 2010, pp. 1647–1651. doi:10.2514/1.J050025

[47] Osgerby, I. T., Smithson, H. K., and Wagner, D. A., "Supersonic Combustion Tests with a Double-Oblique-Shock Scramjet in a Shock Tunnel," *AIAA Journal*, Vol. 8, No. 9, 1970, pp. 1703–1705. doi:10.2514/3.5970

[48] Morgan, R. G., and Stalkerf, R. J., "Shock Tunnel Measurements of Heat Transfer in a Model Scramjet," *Journal of Spacecraft and Rockets*, Vol. 23, No. 5, 1986, pp. 470–475. doi:10.2514/3.25831

[49] Blankson, I. M., Murthy, S. N. B., and Bruno, C., "Scramjet Combustor and Flow Path Scaling," NATO Technical Rept. RTO-TR-AVT-007-V2, Brussels, Belgium, 2012, Chap. 9.

[50] Nagamatsu, H. T., and Martin, E. D., "Combustion Investigation in the Hypersonic Shock Tunnel Driver Section," *Journal of Applied Physics*, Vol. 30, No. 7, 1959, pp. 1018–1021. doi:10.1063/1.1776974

[51] Robinson, M. J., Mee, D. J., and Paull, A., "Scramjet Lift, Thrust and Pitching-Moment Characteristics Measured in a Shock Tunnel," *Journal of Propulsion and Power*, Vol. 22, No. 1, 2006, pp. 85–95. doi:10.2514/1.15978

[52] Pulsonetti, M. V., "Scaling and Ignition Effects in Scramjets," *Proceedings of the 11th Australian Fluid Mechanics Conference*, edited by M. R. Davis, and G. J. Walker, Univ. of Tasmania, Hobart, Tasmania, Dec. 1992, pp. 431–434.

[53] Gnanasekar, S., Ashok, V., Dipankar, D., and Lazar, T. C., "Effect of Connected Pipe Test Conditions on Scramjet Combustor Performance," *International Journal on Aerospace Innovations*, Vol. 1, No. 4, 2009, pp. 159–173. doi:10.1260/175722509790291536

[54] Desikan, S. L. N., Suresh, K., Srinivasan, K., and Raveendran, P. G., "Fast Response Co-Axial Thermocouple for Short Duration Impulse Facilities," *Applied Thermal Engineering*, Vol. 96, No. 5, 2016, pp. 48–56. doi:10.1016/j.applthermaleng.2015.11.074

[55] Bogdanoff, D. W., Zambrana, H. A., and Cavolowsky, J. A., "Reactivation and Upgrade of the NASA Ames 16 Inch Shock Tunnel; Status Report," AIAA Paper 1992-0327, 1992. doi:10.2514/6.1992-327

[56] Mee, D. J., "Uncertainty Analysis of Conditions in the Test Section of the T4 Shock Tunnel," Rept. 4/93, Dept. of Mechanical Engineering, The Univ. of Queensland, Queensland, 1993.

[57] Schramm, J. M., Karl, S., Hannemann, K., and Steelant, J., "Ground Testing of the HyShot II Scramjet Configuration in HEG," AIAA Paper 2008-2547, 2008. doi:10.2514/6.2008-2547

[58] Mateu, M. M., "Study of an Air-Breathing Engine for Hypersonic Flight," Technical Rept., Universitat Polytecnica De Catalunya, Barcelona, Spain, 2013.

Y. Ju
Associate Editor

Downloaded by BIBLIOTHEK DER TU MUENCHEN on July 21, 2018 | http://arc.aiaa.org | DOI: 10.2514/1.J056761